1
2

CMKLR1-targeting peptide tracers for PET/MR imaging of breast cancer

5
6

7

Sarah Erdmann[1], Lars Niederstadt[1], Eva Jolanthe Koziolek[2,3,4], Juan Daniel Castillo Gómez[2], Sonal Prasad[2,3], Asja Wagener[1], Jan Lennart von Hacht[1], Sandy Hallmann[1], Samantha Exner[1], Sebastian Bandholtz[1], Nicola Beindorff[3], Winfried Brenner[2,3,5], Carsten Grötzinger[1,2,5]

12
13
14

[1] Department of Hepatology and Gastroenterology, Molecular Cancer Research Center (MKFZ), Charité – Universitätsmedizin Berlin, Campus Virchow-Klinikum, 13353 Berlin, Germany; [2] Department of Nuclear Medicine, Charité – Universitätsmedizin Berlin, Campus Virchow-Klinikum, 13353 Berlin, Germany; [3] Berlin Experimental Radionuclide Imaging Center (BERIC), Charité – Universitätsmedizin Berlin, Campus Virchow-Klinikum, 13353 Berlin, [4] German Cancer Research Center (DKFZ) Heidelberg, Germany, [5] German Cancer Consortium (DKTK), Berlin, Germany

22
23
24

25

26

Running title: CMKLR1 PET/MRI in a breast cancer xenograft model

28
29

Corresponding author: Dr. Carsten Grötzinger
                Charité - Universitätsmedizin Berlin
                Campus Virchow-Klinikum
                Department of Hepatology and Gastroenterology and
                Molecular Cancer Research Center (MKFZ)
                Augustenburger Platz 1
                D-13353 Berlin
                Germany
                Phone: +49 30 450559488
                Fax: +49 30 45055997
                Email: carsten.groetzinger@charite.de

41

Abstract

42   Molecular targeting remains to be a promising approach in cancer medicine. Knowledge

43   about molecular properties such as overexpression of G protein-coupled receptors

44   (GPCRs) is thereby offering a powerful tool for tumor-selective imaging and treatment of

45   cancer cells. We utilized chemerin-based peptides for CMKLR1 receptor targeting in a

46   breast cancer xenograft model. By conjugation with radiolabeled chelator 1,4,7,10-

47   tetraazacyclododecane-1,4,7,10-tetraacetic acid (DOTA), we obtained a family of highly

48   specific and affine tracers for hybrid *in vivo* imaging with positron emission tomography

49   (PET)/ magnetic resonance (MR) and concomitant biodistribution studies.

Methods

51   We developed five highly specific and affine peptide tracers targeting CMKLR1 by linker-

52   based conjugation of chemerin peptide analogs (CG34 and CG36) with radiolabeled

53   (^{68}Ga) chelator DOTA. Our established xenograft model with target-positive DU4475 and

54   negative A549 tumors in immunodeficient nude mice enabled CMKLR1-specific imaging

55   *in vivo*. Therefore, we acquired small animal PET/MR images, assessed biodistribution by

56   *ex vivo* measurements and investigated the tracer specificity by blocking experiments.

Results

58   The family of five CMKLR1-targeting peptide tracers demonstrated high biological activity

59   and affinity *in vitro* with EC_{50} and IC_{50} values being below 2 nM. Our target-positive

60   (DU4475) and target-negative (A549) xenograft model could be confirmed by *ex vivo*

61   analysis of CMKLR1 expression and binding. After preliminary PET imaging, the three

62   most promising tracers ^{68}Ga-DOTA-AHX-CG34, ^{68}Ga-DOTA-KCap-CG34 and ^{68}Ga-

63   DOTA-ADX-CG34 with apparent DU4475 tumor uptake were further analyzed. Hybrid

64   PET/MR imaging along with concomitant biodistribution studies revealed distinct

2

66   CMKLR1-specific uptake (5.1% IA/g, 4.5% IA/g and 6.2% IA/g 1 h post-injection) of our

67   targeted tracers in DU4475 tumor tissue. More strikingly, the tumor uptake could be

68   blocked by excess of unlabeled peptide (6.4-fold, 7.2-fold and 3.4-fold 1 h post-injection)

69   and further confirmed the CMKLR1 specificity. As our five tracers, each with particular

70   degree of hydrophobicity, showed different results regarding tumor uptake and organ

71   distribution, we identified these three tracers with moderate, balanced properties to be the

72   most potent in receptor-mediated tumor targeting.

73   **Conclusion**

74   With the breast cancer cell line DU4475, we established a model endogenously

75   expressing our target CMKLR1 to evaluate our chemerin-based peptide tracers as highly

76   affine and specific targeting agents. Eventually, we demonstrated the applicability of our

77   ^{68}Ga-labeled tracers by visualizing CMKLR1-positive breast cancer xenografts in PET/MR

78   imaging and thus developed promising theranostics for tumor treatment.

79

80   **Keywords**

81   Tumor targeting, PET tracer, Chemokine-like receptor 1, peptide ligand, breast cancer

82

83

Introduction

84 Molecular targeting remains to be one of the most promising approaches in cancer

85 diagnosis and therapy. Targeted tracers in combination with highly sensitive positron

86 emission tomography (PET) may facilitate early tumor recognition and staging staging as

87 well as therapeutic stratification and response monitoring. While the most widely used

88 PET tracer ^{18}F-fluoro-deoxyglucose (^{18}F-FDG) enables tumor detection by glucose

89 metabolic imaging and hence also visualizes non-neoplastic cells and tissues, tumor-

90 specific targeting is aiming to provide more sensitive and precise imaging results with less

91 non-specific background [1]. Preferred molecular targets are considered to localize at the

92 cell surface or within the extracellular matrix (ECM), as tracers can reach them without

93 crossing the cell membrane. Consequently, transmembrane receptors, transporters and

94 other antigens associated with the cell membrane as well as ECM proteins such as

95 fibronectin or tenascin can be regarded as potential targets [2]. With either high

96 overexpression or even exclusive target expression in tumor cells, appropriately targeted

97 tracers may lead to improved tumor-to-background ratios and thus higher diagnostic

98 sensitivity and specificity.

99 Several G protein-coupled receptors (GPCRs) have been identified as tumor-specific

100 targets. Beside other well-characterized cell surface proteins such as growth factor

101 receptors (e.g. epithelial growth factor receptor, EGFR [3]), transmembrane glycoproteins

102 (e.g. prostate-specific membrane antigen, PSMA [4]) and transmembrane receptors (e.g.

103 integrins [5]), GPCRs have emerged as molecular targets in the field of cancer care [6, 7].

104 Thus, upregulated receptor expression in cancer cells can be utilized for tracer-based

105 tumor imaging, for pharmacological intervention through GPCR signaling modification and

106 for peptide receptor radionuclide therapy (PRRT). Unlike antibodies, small-sized receptor

4

108 ligands such as peptides have a number of advantages regarding their *in vivo* circulation,

109 biodistribution, tumor penetration and low immunogenic potential [8-11].

110 One of the earliest successful receptor-based strategies in cancer targeting was the use

111 of somatostatin analogs (SSA) for diagnostic imaging and treatment of somatostatin

112 receptor-bearing tumors. For human somatostatin receptor (SSTR), a G protein-coupled

113 transmembrane glycoprotein, five subtypes (SSTR1-SSTR5) are known to be expressed

114 in neuroendocrine tumors (NETs) [12, 13]. With a prevalence of 80 to 100% and the

115 highest abundance for SSTR2 expression, NETs of the gastroenteropancreatic tract

116 (75%, compared to 25% NETs in lungs) are suited for SSTR targeting [14, 15]. While [111]In-

117 pentetreotide (^{111}In-DTPA-octreotide) for single photon emission computed tomography

118 (SPECT) was the first SSTR tracer with widespread clinical use [16, 17], ^{68}Ga-DOTATOC

119 (^{68}Ga-DOTA-Tyr[3]-octreotide) for PET and ^{177}Lu-DOTATATE (^{177}Lu-DOTA-Tyr[3]-

120 octreotate) for PRRT have now become available [18-20].

121 Chemokine-like receptor 1 (CMKLR1), a G protein-coupled receptor, and its ligand

122 chemerin are known to be involved in inflammation, adipogenesis and glucose

123 metabolism [21, 22]. Dysregulation of the receptor-ligand system has been linked to

124 several pathologies such as metabolic syndrome and cardiovascular diseases [23, 24].

125 Apart from a study demonstrating recruitment of immune cells and hence an antitumor

126 response in melanoma, the role of the chemoattractant chemerin and its receptors in

127 cancer is largely unknown [25, 26]. Our lab has recently characterized CMKLR1 as a

128 target overexpressed in breast cancer, esophageal squamous cell carcinoma (ESCC) and

129 pancreatic adenocarcinoma (manuscript in preparation). Increased CMKLR1 expression,

130 chemerin-mediated tumor cell migration and invasion in ESCC were also found by Kumar

131 et al. [27]. Likewise, CMKLR1 has been implicated in neuroblastoma proliferation [28],

132   hepatocellular carcinoma metastasis [29] and migration/invasion of gastric cancer [30].

133   CMKLR1 may therefore be a promising target for molecular imaging and targeted

134   radionuclide therapy in overexpressing tumor entities. This study evaluated the potential

135   of a family of novel CMKLR1 peptide-DOTA tracers for PET/MR imaging in a breast

136   cancer animal model.

137

138 **Material and Methods**

139 *Peptides*

140 All peptides and DOTA-peptide conjugates were from peptides&elephants (Hennigsdorf,

141 Germany). They were analyzed by mass spectrometry to confirm the presence of the

142 correct molecular mass. Peptides and peptide conjugates were used at a purity of greater

143 than 95%. Analysis data for peptides and peptide conjugates have been deposited in an

144 open data repository for public access: http://doi.org/10.5281/zenodo.2591417

145 *Cell culture*

146 For *in vitro* analysis, HEK293a stably transfected with huCMKLR1 and $G_{\alpha 16}$ were used.

147 For the *in vivo* mouse model, the human breast cancer cell line DU4475 with endogenous

148 CMKLR1 expression and the target-negative human lung carcinoma cell line A549 were

149 used. All cell lines were obtained from ATCC/LGC Standards (Wesel, Germany) and were

150 cultured in RPMI1640 medium containing 10% fetal bovine serum (both from Biochrom,

151 Berlin, Germany) and, in case of transfected cells, selection agents G418 (Biochrom) and

152 zeocin (Invitrogen, Carlsbad, USA).

153 *Xenografts*

154 For *in vivo* experiments, at least 8-week-old female athymic NMRI-*Foxn1^{nu}/Foxn1^{nu}* mice

155 (Janvier Labs, Saint-Berthevin, France) were used. Animal care followed institutional

156 guidelines and all experiments were approved by local animal research authorities. For

157 the generation of tumor xenografts, 5×10^6 cells of both DU4475 and A549 cells were

158 inoculated subcutaneously into the left and right shoulder, respectively (1:1 PBS/Matrigel

159 Basement Membrane Matrix High Concentration, Corning, Corning, USA). Tumors were

160 allowed to grow for two to four weeks (tumor volume > 100 mm^3) after cell inoculation.

161 *Immunofluorescence*

162   For immunofluorescent staining of tumor tissue, the frozen xenografts were embedded in

163   Tissue-Tek O.C.T Compound (Sakura Finetek, Torrance, USA), trimmed by cryostat (12-

164   18 µm) and transferred on glass slides (Superfrost, Thermo Fisher Scientific, Waltham,

165   USA). Xenograft sections were fixed with 1:1 methanol/acetone for two minutes and air-

166   dried. After washing with PBS (Biochrom, Berlin, Germany), sections were blocked with

167   2% milk powder (blotting grade; Bio-Rad Laboratories, Hercules, USA) in PBS for

168   30 minutes. Sections were incubated with the primary anti-CMKLR1 antibody developed

169   in our lab (#21-86; polyclonal from rabbit, immunogenic peptide sequence:

170   SSWPTHSQMDPVGY; 3 µg/mL diluted in 0.1% BSA in PBS) in a wet chamber over night

171   at 4 °C. After washing, sections were incubated with the secondary antibody goat-anti-

172   rabbit-Cy2 (Jackson ImmunoResearch, West Grove, USA; 7.5 µg/mL diluted in 0.1% BSA

173   in PBS) for one hour. After washing with TBS, nuclei staining with 1 µM SytoxOrange

174   (Thermo Fisher Scientific, Waltham, USA) in TBS followed. Finally, the cryosections were

175   fixed with 96% ethanol for two minutes, embedded with Immu-Mount (Thermo Fisher

176   Scientific, Waltham, USA) and analyzed with a confocal laser-scanning microscope

177   (LSM510, Carl Zeiss, Jena, Germany).

178   *Calcium mobilization assay*

179   Optical ViewPlate 96-well microplates (PerkinElmer, Waltham, USA) were coated with

180   poly-D-lysine (10 µg/mL, 50 µL/well) for 30 minutes at 37 °C, washed with PBS and air

181   dried before seeding 40,000 HEK293a huCMKLR1 $G_{\alpha 16}$ cells per well. The next day, cells

182   were starved with serum-free medium for 30 minutes and incubated with loading medium

183   consisting of serum-free medium with 2.5 mM probenicid (Sigma-Aldrich, St. Louis, USA)

184   and 2 µM Fluo-4 AM (Thermo Fisher Scientific, Waltham, USA). After a loading time of 45

185   minutes, cells were washed with 100 µL C1 buffer (130 mM NaCl, 5 mM KCl, 10 mM Na-

8

186   Hepes, 2 mM $CaCl_2$, 10 mM glucose) followed by 20 minutes of incubation in the dark.

187   After another washing and incubation cycle, the cell plate was placed into the CellLux

188   Calcium Imaging System (PerkinElmer, Waltham, USA) and the assay was performed

189   automatically according to the following protocol. After a baseline measurement for

190   30 seconds, the ligands (prepared in C1 buffer with 0.5% BSA in double concentration

191   and pipetted in a U-bottom plate) were added on top of the cells and the fluorescence

192   intensity was recorded for a further 60 seconds. Obtained raw data were analyzed using

193   AssayPro (PerkinElmer, Waltham, USA). After spatial uniformity correction, maximum

194   response values (F) were normalized to baseline values (F_0) of each well using the

195   following equation: response = $\Delta F/F_0$ = $(F - F_0)/F_0$.

196   *Iodination of chemerin-9*

197   Radioactive iodination of chemerin-9 was performed by the chloramine T method [31]. For

198   labeling, 10 nmol of chemerin-9 in 25 µL iodination buffer (0.5 M sodium phosphate,

199   pH 7.4) were mixed with 1 mCi carrier-free $Na^{125}I$ (NEZ033L010MC, PerkinElmer,

200   Waltham, USA) in an HPLC glass vial with microvolume insert. The reaction was started

201   by adding 4 µL chloramine T (1 mg/mL in water). After 20-30 seconds, 4 µL of sodium

202   metabisulfite (2 mg/mL in water) were added to stop the iodination. HPLC purification was

203   performed to separate unlabeled from labeled radioactive peptide on an Agilent ZORBAX

204   300 Extend-C18 column using a gradient from 20 to 50% acetonitrile (+0.1% TFA) against

205   water (+0.1% TFA) for 20 minutes. First, 1-2 µL of the reaction mixture were preanalyzed

206   to determine the retention time of the radioactive peptide. This fraction was then collected

207   during the main run, diluted with radioactive binding buffer to prevent radiolysis, aliquoted

208   and stored at -20 °C.

209   *Competitive binding studies*

210 Competitive binding studies were performed with cell membrane preparations. Therefore,

211 cellular monolayer cultures were washed with pre-warmed PBS and dissociated in ice-

212 cold PBS with 5 mM EGTA (Carl Roth, Karlsruhe, Germany) with the help of a cell scraper.

213 Tumor tissue was homogenized with a rotor-stator homogenizer (Ultra-Turrax T8, IKA-

214 Werke, Staufen, Germany) in ice-cold PBS with 5 mM EGTA. Both, cell and tissue

215 homogenates were centrifuged for ten minutes (4 °C, 200 x g), and supernatants were

216 discarded. Pellets were resuspended in 5 mL of membrane isolation buffer (5 mM TrisHCl

217 pH 7.6, 5 mM $MgCl_2$, 1 mM EGTA, protease inhibitor cocktail cOmplete [Roche Applied

218 Science, Penzberg, Germany]) with a glass dounce tissue grinder (Wheaton, Millville,

219 USA) and further homogenized by moving the pestle up and down (approx. 30 times).

220 After centrifugation for 30 minutes (4 °C und 40.000 g), the process was repeated, before

221 cell and tissue homogenates were resuspended in 1 mL membrane isolation buffer,

222 aliquoted and stored at -80 °C. For competitive binding, 5 µg of isolated membrane in

223 25 µL binding buffer (50 mM 4-(2-hydroxyethyl)-1-piperazineethanesulfonic acid (HEPES)

224 pH 7.4, 5 mM $MgCl_2$, 1 mM $CaCl_2$, 0.5% BSA, protease inhibitor cocktail cOmplete) were

225 incubated with increasing concentrations of non-radioactive peptide (2-fold concentrated

226 in 50 µL) and 100,000 cpm of ^{125}I-chemerin-9 (in 25 µL binding buffer). After one hour of

227 incubation at 37 °C, the mixture was transferred to 96-well filter plates (MultiScreen$_{HTS}$ FB

228 Filter Plate 1.0 µm, Millipore, Billerica, USA), unbound peptide was withdrawn by suction

229 and the plate was washed four times with cold washing buffer (50 mM Tris-HCl pH 7.4,

230 125 mM NaCl, 0.05% BSA). After drying the filter plate, 40 µL scintillation cocktail (Ultima

231 Gold F, Perkin Elmer, Waltham, USA) per well was added and radioactivity was measured

232 by liquid scintillation counting (MicroBeta^2 Microplate Counter, PerkinElmer, Waltham,

233 USA).

10

Radiochemical labelling

234

235 Radiolabeling experiments were performed on a Modular Lab PharmTracer synthesis

236 module (Eckert & Ziegler, Berlin, Germany) which allows fully automated cassette-based

237 labeling of gallium tracers utilizing a pharmaceutical grade ^{68}Ge/^{68}Ga generator

238 (GalliaPharm, 1.85 GBq, good manufacturing practice (GMP)-certified; Eckert & Ziegler

239 GmbH, Berlin, Germany). Cassettes were GMP-certified and sterile. They were used

240 without pre-conditioning of the cartridges. The gallium generator was eluted with aqueous

241 HCl (0.1 M, 7 mL) and the eluate was purified on an ion-exchange cartridge followed by

242 elution using 1 mL of 0.1 M HCl in acetone. The peptide-DOTA conjugate (50 µg from a

243 stock solution 1 mg/mL in 10% DMSO, 90% water) was mixed with 500 µL 0.1 M HEPES

244 buffer (pH 7) and heated for 500 s at 95 °C. After the reaction, the mixture was passed

245 through a C-18 cartridge for purification and the tracer was eluted from the cartridge with

246 ethanol. For injection, the resulting solution was diluted with saline to ≤ 10% ethanol.

PET/MR imaging

247

248 Positron emission tomography (PET)/magnetic resonance imaging (MRI) (1 Tesla

249 nanoScan PET/MRI, Mediso, Hungary) was performed at the Berlin Experimental

250 Radionuclide Imaging Center (BERIC), Charité – Universitätsmedizin Berlin. A dedicated

251 mouse whole-body coil was used for RF-transmission and signal receiving. Mice were

252 anesthetized with general anaesthesia (1-2% isoflurane/0.5 L/min oxygen). Body

253 temperature was maintained at 37 °C during the time of imaging by using a heated bed

254 aperture. Anatomic whole-body MRI scans were acquired using a high-resolution T2-

255 weighted 2D fast spin echo sequence (T2 FSE 2D) with the following parameters: TR =

256 8700 ms; TE = 103 ms; slice thickness/gap = 1.1 mm/ 0.1 mm; matrix = 256 x 256 mm;

11

257 external averages = 5 and number of excitations = 2. PET scans in list mode were

258 acquired either for 30 minutes one and two hours after intravenous injection or for 90

259 minutes of dynamic imaging starting directly before injection of 0.15 mL of tracer,

260 corresponding to a ^{68}Ga activity of approximately 20 MBq for static 1 h-images and 2 h-

261 images and 15 MBq for kinetic imaging. To determine the effect of unlabeled ligand on

262 the tumor uptake, 200 nmol CG34 peptide (50-fold excess) was co-injected. Static PET

263 images were reconstructed from the raw data as one image (1 x 1800 s) and dynamic

264 PET images were reconstructed with the image sequence 9 x 600 s. The uptake value

265 (kBq/cm^3) in the tumor tissue was determined by manual contouring of a volume of interest

266 (VOI) of the PET images using PMOD 3.610 (PMOD Technologies, Zürich, Switzerland).

267 *Biodistribution studies*

268 Tumor-bearing mice were injected with approximately 10 MBq of ^{68}Ga-DOTA-peptide to

269 the tail vein via a catheter. Mice were sacrificed and dissected one or two hours after

270 injection. Tumor, blood, stomach, pancreas, small intestine, colon, liver, spleen, kidney,

271 heart, lung, muscle and femur samples were weighed and uptake of radioactivity was

272 measured by a gamma counter. To determine the effect of unlabeled ligand on the tumor

273 uptake, 200 nmol CG34 peptide (100-fold excess) was co-injected.

274 *Statistical analysis*

275 All statistical analyses were performed using GraphPad Prism 5.04. EC$_{50}$/IC$_{50}$ values were

276 determined by nonlinear sigmoidal curve fitting with variable slope setting, and normalized

277 response for competitive binding results. Multiple group comparisons were done by a two-

278 way ANOVA and Bonferroni post hoc test. All presented data are based on independent

279 experiments. Normalizations and statistics are further defined in each figure legend.

280 *Data availability*

281   Numerical data for all experiments (xlsx file) have been deposited in an open data

282   repository for public access: http://doi.org/10.5281/zenodo.2591417

283

284   **Results**

285

286   **Characterization of an endogenously CMKLR1-expressing tumor mouse model**

287   As models for tracer testing, the human breast cancer cell line DU4475, which

288   endogenously expresses high levels of CMKLR, and the target-negative human lung

289   cancer cell line A549 were chosen to induce subcutaneous xenograft tumors in nude mice.

290   Analysis of *ex vivo* tumor tissue confirmed CMKLR1 expression in DU4475 xenografts by

291   immunostaining, whereas A549 tumors showed no detectable antigen (Figure 1A). To

292   confirm presence of receptor protein in these xenograft tissues with an independent

293   method, radioligand binding studies were performed on membrane preparations of

294   cultured cells and *ex vivo* tissue (Figure 1B). Receptor binding of ^{125}I-labeled chemerin-9

295   in DU4475 cell membrane preparations (*in vitro*) led to values around 200 cpm

296   (assessment of radioactivity by liquid scintillation counting) which could be significantly

297   blocked (approx. 80 cpm) by an excess of the unlabeled peptide (1 µM). Membranes

298   isolated from DU4475 tumors (ex vivo) bound less labeled peptide (approx. 115 cpm) but

299   still exhibited specific binding, as 1 µM chemerin-9 clearly displaced about 50% of the

300   bound activity (60 cpm). In contrast, membrane preparations from A549 cells xenograft

301   tumors showed no specific binding.

302

303   **Characterization of high potency, high affinity CMKLR1-targeting peptide-DOTA**

304   **conjugates**

305   Chemical design of five tracers for CMKLR1 targeting involved two peptide analogs of the

306   natural CMKLR1 ligand chemerin (CG34 or CG36) that were attached to the chelator

307   1,4,7,10-tetraazacyclododecane-1,4,7,10-tetraacetic acid (DOTA) via one of four different

14

308 chemical linkers: 4,7,10-trioxatridecan-succinamic acid (TTDS), 6-aminohexanoic acid

309 (AHX), N-ε-capryloyl-lysine (KCap) and 10-aminodecanoic acid (ADX) (Figure 2A). Due

310 to their chemical composition, both peptide analogs as well as the four linkers exhibit

311 distinct characteristics such as different length and hydrophobicity. In Figure 2A, these

312 conjugate components are depicted in different colors (reddish colors indicate more

313 hydrophobic properties and greenish colors more hydrophilicity).

314

315 *In vitro* characterization of the probes was realized by activity and radioligand binding

316 studies in HEK293a cells stably transfected with CMKLR1. Ligand-induced receptor

317 activation as intracellular Ca^{2+} flux was quantified in an intracellular calcium mobilization

318 assay (Figure 2B). Concentration-response profiles for all five tracers were determined

319 and EC_{50} values were calculated. In comparison to the unconjugated peptide analog

320 CG34 (EC_{50} 0.4 nM), the TTDS-linked DOTA conjugate of CG34 had a slightly higher

321 EC_{50} value of 1.51 nM. Receptor affinity was assessed by competitive radioligand binding

322 studies and resulting IC_{50} values were derived (Figure 2C). Furthermore, DOTA

323 conjugates were labeled with non-radioactive gallium (^{nat}Ga) to investigate a potential

324 impact of metal ion complexation on binding affinity. For DOTA-TTDS-CG34, gallium

325 labeling barely had an effect on receptor binding (IC_{50} value approximately 0.6 nM). As

326 the unconjugated peptide CG34 exhibited an IC_{50} of 1.0 nM, conjugation with DOTA had

327 even increased its binding affinity. Figure 2D summarizes all EC_{50} and IC_{50} values of the

328 five DOTA peptide conjugates. All CG34 conjugates showed EC_{50} values within the low

329 nanomolar range of approx. 0.6 – 1.5 nM, thus, 1.6- to 3.75-fold higher values for receptor

330 activation than for the unconjugated peptide. However, for receptor binding the IC_{50} values

331 were similar to the value for CG34 or even lower (subnanomolar range: approx.

15

332   0.3 – 1.0 nM) and cold gallium labeling did not adversely affect the affinity. Compared to

333   the activating potency (EC_{50} 0.9 nM) and binding affinity (IC_{50} 0.1 nM) of the unconjugated

334   peptide CG36, the DOTA-AHX-CG36 probe exhibited only slightly higher values (EC_{50}

335   1.53 nM, IC_{50} w/o ^{nat}Ga 0.13 nM and w/ ^{nat}Ga 0.13 nM).

336

337   ***In vivo* PET/MR imaging and biodistribution studies demonstrate specific tracer**

338   **uptake in CMKLR1-expressing tumors**

339   An initial PET study was performed to estimate the *in vivo* behavior of the five tracer

340   conjugates after ^{68}Ga labeling. Tumor-bearing mice received an intravenous injection of

341   approximately 20 MBq radiotracer and were imaged for 30 minutes starting one hour post-

342   injection in the PET/MRI scanner. Figure 3 shows *in vivo* PET images of the five tracers,

343   depicted with hydrophobicity increasing from left to right. The most hydrophilic tracer ^{68}Ga-

344   DOTA-TTDS-CG34 accumulated mainly in the kidneys (Figure 3A, yellow arrow) with no

345   clear DU4475 tumor uptake (right shoulder) compared to the general background. With

346   ^{68}Ga-DOTA-AHX-CG34, tumor-to-background signal was found to be higher (Figure 3B,

347   white arrow) and accompanied by less kidney uptake. The tracer uptake within the target-

348   positive tumor on the right shoulder was even more enhanced with KCap as linker (Figure

349   3C, white arrow). The most hydrophobic CG34 tracer, with ADX as a linker, also led to

350   specific tumor uptake (Figure 3D, white arrow), but also high kidney (yellow arrow) and

351   apparent liver uptake (red arrow). For the tracer ^{68}Ga-DOTA-AHX-CG36, kidney and liver

352   signals were high but almost no tumor uptake could be detected (Figure 3E). Based on

353   these initial *in vivo* findings, the three most promising tracers ^{68}Ga-DOTA-AHX-CG34,

354   ^{68}Ga-DOTA-KCap-CG34 and ^{68}Ga-DOTA-ADX-CG34 were further analyzed. In addition

355   to PET/MRI scans, *ex vivo* biodistribution studies were performed.

16

356

357   *In vivo* hybrid imaging with ^{68}Ga-DOTA-KCap-CG34 and ^{68}Ga-DOTA-ADX-CG34 using

358 the PET/MRI scanner enabled not only functional PET analysis of the tracers but also

359 allowed to gain anatomical insights into the tumor tissue and volume by high-resolution

360 T2-weighted MR imaging (upper panels, Figure 4). As seen in the T2-weigthed images,

361 both tumors (A549 on the left and DU4475 on the right shoulder) were of comparable size,

362 tissue characteristics and vascularization. The KCap-linked radiotracer apparently

363 accumulated in the DU4475 tumor and in kidneys one hour post-injection with decreasing

364 PET signals after two hours. In contrast, no clear A549 tumor signal could be detected

365 (upper panel, Figure 4A). In addition to *in vivo* imaging, tumor-bearing mice were injected

366 with approximately 10 MBq of radiotracer and sacrificed after one and two hours,

367 respectively. By *ex vivo* measurement, tissue radioactivity was calculated as percentage

368 of injected activity per gram tissue (% IA/g). After one hour, ^{68}Ga-DOTA-KCap-CG34 led

369 to a DU4475 tumor uptake of about 4.5% IA/g and was 2-fold less in the A549 tumor with

370 approx. 2.3% IA/g. Furthermore, higher values were measured for spleen (approx. 4.9%

371 IA/g) and, due to the predominant renal excretion of peptides, for kidneys (approx. 5.8%

372 IA/g). The DU4475 uptake decreased to approx. 2.9% IA/g, whereas the kidney signal

373 increased up to approx. 6.5% IA/g two hours post-injection (lower panel, Figure 4A). For

374 ^{68}Ga-DOTA-ADX-CG34, the PET signal in DU4475 tumor and kidneys was comparatively

375 stronger one and two hours post-injection than the uptake of ^{68}Ga-DOTA-KCap-CG34 and

376 there was also an additional distinct liver uptake of the radiotracer (upper panel, Figure

377 4B). These higher organ uptakes were confirmed by biodistribution data (lower panel,

378 Figure 4B). In addition to overall higher values one hour after injection, liver (approx.

379 14.2% IA/g), kidney (10.3% IA/g) and spleen (7.8% IA/g) uptakes were the most profound

17

380   off-target effects. However, with approx. 6.2% IA/g for CMKLR1-positive DU4475 tumors

381   and approx. 2.7% IA/g for target-negative A549 tumors, PET results and tracer specificity

382   could be confirmed. After two hours, DU4475 uptake declined by 1.5-fold to approx. 4.2%

383   IA/g and a distinct liver uptake (approx. 12.5% IA/g) persisted. Kinetic measurements of

384   tracer concentration in tumors, kidneys and liver demonstrated a delayed kidney peak for

385   ^{68}Ga-DOTA-KCap-CG34, the most hydrophobic molecule, with rapid washout from

386   kidneys for both ^{68}Ga-DOTA-AHX-CG34 and ^{68}Ga-DOTA-ADX-CG34 (Figure S2). While

387   the other two tracers showed a small decline in the DU4475 tumor, ^{68}Ga-DOTA-ADX-

388   CG34 appeared to gain in tumor activity until 90 min p.i.

389

390   **Receptor blocking studies verify tracer specificity**

391   For further investigation of CMKLR1 specificity of the radiotracers, blocking experiments

392   were carried out. To examine whether tracer binding to the tissues could be displaced,

393   PET/MR imaging was performed twice with the same animal, once with and once without

394   an excess of unlabeled peptide. In parallel, biodistribution experiments under blocking

395   conditions (excess of unlabeled peptide) were performed to confirm PET results

396   independently in a quantitative manner.

397

398   Figure 5 shows representative results of *in vivo* receptor blocking experiments with [68]Ga-

399   DOTA-AHX-CG34. PET/MR imaging without excess of the unconjugated and unlabeled

400   peptide CG34 showed DU4475 tumor and kidney signals one hour post-injection (Figure

401   5A). However, co-injection of 200 nmol CG34 (50-fold excess) led to a complete loss of

402   tumor uptake and a highly enhanced kidney signal (Figure 5B). The tracer biodistribution

403   one hour after injection without competing CG34 clearly demonstrated the distinct

18

404   DU4475 tumor uptake (approx. 5.1% IA/g) and the high kidney (approx. 6.5% IA/g) and

405   spleen (approx. 6.3% IA/g) values (Figure 5C). CMKLR1 blocking with an excess of CG34

406   led to an overall low tissue and organ radioactivity except for strong kidney uptake (8.6%

407   IA/g) and excretion into the urinary bladder. The tracer uptake within DU4475 tumors could

408   be blocked by a factor of 6.4 to approximately 0.8% IA/g (Figure 5D).

409

19

410 A summary of all biodistribution data including calculated tissue radioactivity ratios for the

411 three most promising tracers ^{68}Ga-DOTA-AHX-CG34, ^{68}Ga-DOTA-KCap-CG34 and ^{68}Ga-

412 DOTA-ADX-CG34 is presented in Table 1. Use of these CMKLR1 tracers resulted in

413 distinct target-specific DU4475 tumor uptake with 5.1% IA/g (^{68}Ga-DOTA-AHX-CG34),

414 4.3% IA/g (^{68}Ga-DOTA-KCap-CG34) and 6.2% IA/g (^{68}Ga-DOTA-ADX-CG34). All three

415 of them showed favorable tumor-to-kidneys ratios with 0.9, 0.7 and 0.8. CMKLR1

416 specificity could be proven by 1.8-fold (5.1 vs. 3.0% IA/g), 1.9-fold (4.3 vs. 2.3% IA/g) and

417 2.3-fold (6.2 vs. 2.7% IA/g) higher uptake in CMKLR1-positive DU4475 tumors than in

418 target-negative A549 tumors one hour post-injection. In addition, receptor blocking by co-

419 injection of an excess of unlabeled chemerin peptide diminished specific tracer binding by

420 6.4-fold (5.1 vs. 0.8% IA/g), 7.2-fold (4.3 vs. 0.6% IA/g) and 3.4-fold (6.2 vs. 1.8% IA/g).

421 The most stable and durable tumor uptake was achieved by ^{68}Ga-DOTA-AHX-CG34 with

422 4.9% IA/g (approx. 96% of the 1 h-value) after two hours, whereas uptake of the KCap-

423 linked (approx. 67%) and ADX-linked (approx. 68%) tracers declined faster within two

424 hours after injection. The highest overall non-tumor uptake values were seen with ^{68}Ga-

425 DOTA-ADX-CG34, with considerable liver (14.2% IA/g) and kidney (10.3% IA/g) uptake

426 and hence, the lowest tissue radioactivity ratios for the DU4475 tumor.

427

20

Discussion and Conclusions

The purpose of this study was to evaluate a family of five novel CMKLR1 tracers for their capacity to generate target-specific signals in a breast cancer xenograft mouse model. To the best of our knowledge, this is the first report of CMKLR1 *in vivo* imaging. Although known for its role in inflammation and metabolic regulation for many years, CMKLR1 and its chemokine-like ligand chemerin were only recently recognized as modulators of tumor proliferation and expansion. While other labs have reported overexpression and functional involvement of CMKLR1 in esophageal squamous cell carcinoma, hepatocellular carcinoma, neuroblastoma and gastric cancer [27-30], we have recently found CMKLR1 overexpression in breast cancer and pancreatic adenocarcinoma and have consequently developed two peptide analogs of chemerin for use in receptor-mediated tumor targeting (manuscript in preparation). These peptide analogs were based on chemerin-9, which has full agonistic activity towards the receptor CMKLR1 and corresponds to the C-terminal nine amino acids of processed chemerin [32]. In a previous study, we have shown the potential to generate stable and potent chemerin-9 analogs by the introduction of D-amino acids via an evolutionary algorithm [33]. The resulting peptide analogs showed improved properties concerning receptor activation, binding affinity and metabolic stability. In this study, we have made use of such analogs as components of chelator conjugates to do PET/MR imaging in a breast cancer xenograft mouse model.

The suitability of the animal model with CMKLR1-positive DU4475 and CMKLR1-negative A549 xenograft tumors was confirmed by immunofluorescence staining and radioligand binding studies. As expression of proteins in cells may change upon transfer from the

21

451 culture dish monolayer to three-dimensional subcutaneous xenograft tumor tissue in mice,

452 we investigated CMKLR1 expression in tumor tissue. Thereby, overexpression as well as

453 ligand binding were established for DU4475 tumors while A549 tumors were confirmed as

454 a negative control. The moderate tracer uptake seen in the latter is probably due to

455 unspecific mechanisms, such as the enhanced retention and permeability effect or blood

456 pool activity.

457 In the design of our tracers, we followed the hypothesis that tumor uptake and

458 biodistribution may depend on a balance of hydrophobic and hydrophilic properties within

459 the molecule. Therefore, we chose not only to make use of a more hydrophilic and a more

460 hydrophobic CMKLR1 peptide ligand analog, but also to take advantage of different

461 linkers to introduce a varying degree of hydrophobicity into the conjugates. As DOTA with

462 its four carboxylic groups confers rather strong hydrophilic features, we chose to

463 compensate this with mainly hydrophobic linker moieties: 6-aminohexanoic acid (AHX),

464 N-ε-capryloyl-lysine (KCap) and 10-aminodecanoic acid (ADX). Only one linker displayed

465 hydrophilic properties: the PEG-like 4,7,10-trioxatridecan-succinamic acid (TTDS)

466 (Figure 2A). A set of five resulting DOTA peptide conjugates was tested *in vitro* prior to

467 the animal study. Of note, all these tracers proved to be of high affinity and functional

468 activity, with IC_{50} and EC_{50} values being below 2 nM (Figure 2D). Affinity also did not

469 change significantly upon complexation of DOTA with non-radioactive gallium, and if so,

470 IC_{50} values even decreased. This was in many ways unexpected as we and others had

471 often experienced an impairment of the binding and activating capacity of ligands upon

472 conjugation with a linker and a reporter such as a chelator or dye molecule [34-37].

473 Likewise, the affinity of such a conjugate may be affected by the coordination of a

22

474   radiometal ion [38]. The structural requirements of chemerin analogs binding to CMKLR1

475   obviously allow for a broad variety of additions to the N-terminus of the nonameric peptide.

476   Even though the two most potent conjugates were the ones with the shortest linkers (AHX

477   and ADX), differences were small and a significant systematic influence of linker

478   hydrophobicity or length on affinity or activity was not observed.

479   The initial PET studies using all five tracers revealed a clear difference regarding tumor

480   uptake and biodistribution: the most hydrophilic conjugate (^{68}Ga-DOTA-TTDS-CG34) and

481   the most hydrophobic conjugate (^{68}Ga-DOTA-AHX-CG36) both showed lower tumor

482   uptake and higher kidney uptake than the three conjugates with balanced hydrophilicity in

483   the molecule (Figure 3). This was also confirmed by results from biodistribution

484   experiments: for both tracers, there was no clear difference in uptake between target-

485   positive and target-negative tumor (Figure S1 and Table S1). These results may indicate

486   the validity of our hypothesis that sufficient and specific tumor uptake may be achieved

487   best using a conjugate with moderate, balanced hydrophilicity. Both highly hydrophobic

488   and strongly hydrophilic tracers may primarily yield unspecific uptake in kidney and liver.

489   By peptide optimization and conjugation, we were able to obtain a family of five high-

490   potency, high-affinity molecular probes for further *in vivo* application as radioactive

491   tracers. In addition to PET/MRI scans one and two hours post-injection, *ex vivo*

492   biodistribution studies were performed to assess quantitative values for tissue uptake.

493   Utilizing a breast-cancer xenograft mouse model, PET/MRI and concomitant

494   biodistribution studies revealed the specificity of our chemerin-based radiotracers by

495   distinct PET signals and uptake values of CMKLR1-positive DU4475 tumors compared to

496   no PET visibility and low tumor radioactivity values of target-negative A549 tumors.

23

497   Kidney uptake often limits therapeutic use of tracers. For the three best tracers described

498   in this study, renal uptake was between 5.8 to 10.3% IA/g, resulting in favorable tumor-to-

499   kidney ratios of 0.7 to 0.9 at one hour post injection. Further evidence for the specificity of

500   the tracer was obtained in a blocking experiment with an excess of non-labeled peptide

501   (Figure 5). As obvious from both PET/MR images as well as biodistribution data, this

502   excess strongly reduced uptake of the tracer ^{68}Ga-DOTA-AHX-CG34 in CMKLR1-positive

503   DU4475 tumors, indicating displacement of the radioligand from its receptor. The lower

504   uptake observed in other organs probably also corresponds to tracer displacement from

505   chemerin receptors known to be expressed there (e.g. lung, spleen) [21, 39]. The dynamic

506   PET scan of ^{68}Ga-DOTA-AHX-CG34 showed faster background/off-target clearance as

507   well as fast and stable accumulation at tumor sites. Whereas higher hydrophobicity of

508   KCap and ADX led to delayed and prolonged kidney uptake, possibly due to plasma

509   protein binding or metabolization in the liver (Figure S2).

510   While a tumor uptake of 4-6% represents a promising targeting result for these first

511   CMKLR1 tracers, several options for an improvement remain. One current limitation,

512   especially for an application in peptide receptor radionuclide therapy (PRRT), is the fast

513   elimination of the signal from the target-positive tumor. According to biodistribution data,

514   the signal decrease between one hour and two hours in DU4475 tumors was about 25-

515   70%. Although the underlying peptide analogs have been selected for their improved

516   stability in *in vitro* protease degradation assays, a degradation due to proteolytic activity

517   in circulation and target tissue may play a role. Similarly, fast excretion via the renal

518   pathway, as well as hepatic degradation (e.g. ^{68}Ga-DOTA-ADX-CG34) may create

519   unfavorable distribution kinetics. The precise causes for this rapid decrease in tumor

520   signal will have to be determined in subsequent studies. Biochemical isolation and

521   analysis of tracer metabolites from the animal's circulation may provide a means of

522   clarifying the underlying mechanism.

Abbreviations

% IA/g: percent injected activity per gram tissue; ^{18}F-FDG: ^{18}F-fluoro-deoxyglucose; ADX: 10‑aminodecanoic acid; AHX: 6-aminohexanoic acid; BERIC: Berlin Experimental Radionuclide Imaging Center; BSA: bovine serum albumin; CG34: chemerin analog with amino acid sequence Y-Cha-Hyp-G-Cit-F-a-Tic-S; CG36: chemerin analog with amino acid sequence Y-Cha-P-G-M-Y-A-F-f; Chem9: chemerin-9; CMKLR1: chemokine-like receptor 1; DMSO: dimethyl sulfoxide; DOTA: 1,4,7,10-tetraazacyclododecane-1,4,7,10-tetraacetic acid; DTPA: diethylenetriaminepentaacetic acid; EC_{50}: half maximal effective concentration; ECM: extracellular matrix; EGFR: epithelial growth factor receptor; EGTA: ethylene glycol-bis(β-aminoethyl ether)-N,N,N′,N′-tetraacetic acid; ESCC: esophageal squamous cell carcinoma; G418: geneticin; GMP: good manufacturing practice; GPCR: G protein-coupled receptor; HEPES: 4-(2-hydroxyethyl)-1-piperazineethanesulfonic acid; HPLC: high-performance liquid chromatography; IC_{50}: half maximal inhibitory concentration; KCap: N-ε-capryloyl-lysine; MRI: magnetic resonance imaging; NET: neuroendocrine tumor; NMRI: Naval Medical Research Institute; PBS: phosphate-buffered saline; PEG: polyethylene glycol; PET: positron emission tomography; PRRT: peptide receptor radionuclide therapy; PSMA: prostate-specific membrane antigen; RPMI1640: Roswell Park Memorial Institute medium 1640; SD: standard deviation; SEM: standard error of the mean; SSA: somatostatin analog; SSTR: somatostatin receptor; T2 FSE 2D: high-resolution T2-weighted 2D fast spin echo sequence; TBS: tris-buffered saline; TE: echo time; TFA: trifluoroacetic acid; TR: repetition time; TTDS: 4,7,10-trioxatridecan-succinamic acid; VOI: volume of interest

26

Author Contributions

Conception and design: S.E., C.G. Development of methodology: S.E., C.G. Acquisition

of data: S.E., L.N., E.J.K., J.D.C.G., S.P., A.W., J.L.v.H., S.H., S.E., S.B. Analysis and

interpretation of data: S.E., C.G. Writing, review, and/or revision of the manuscript: S.E.,

E.J.K., N.B., W.B., C.G. Study supervision: W.Br., C.G.

Competing interests

The authors have declared that no competing interests exist.

27

554   **Figure Legends**

555

556   **Figure 1: Characterization of the xenograft tumor model.** Breast cancer DU4475 and

557   lung cancer A549 cells were employed to establish a xenograft model with both CMKLR1-

558   positive and -negative tumor. **(A)** Immunostaining of xenograft cryosections revealed

559   CMKLR1 immunostaining (green) in DU4475 *ex vivo* tissue whereas the A549 tumor

560   showed no signal. (blue: cell nuclei; bar = 50 μm) **(B)** Competitive radioligand binding

561   studies with ^{125}I-labeled chemerin-9 showed specific binding to DU4475 cell membranes

562   (*in vitro*) and xenograft tumor membranes (*ex vivo*), which could be blocked by 1 μM

563   unlabeled ligand (Chem9). In contrast, A549 cells showed no and A549 xenografts only

564   minor binding. Data were obtained from at least three independent experiments and

565   values are indicated as means ± SEM. (**** P < 0.0001)

566

567   **Figure 2: Characterization of DOTA peptide conjugates regarding their functionality**

568   **and affinity. (A)** The chelating agent 1,4,7,10-tetraazacyclododecane-1,4,7,10-

569   tetraacetic acid (DOTA) was conjugated to the N-terminus of one of the two optimized

570   chemerin peptide analogs, CG34 and CG36, by one of the four chemical linkers. **(B)** By

571   functional Ca^{2+} mobilization assay, the concentration-response curve for the TTDS-linked

572   CG34 conjugate could be determined and the resulting EC_{50} value (1.51 nM) confirmed

573   its high receptor-activating potency. Response data are presented as mean ± SEM of

574   three independent experiments. **(C)** Ligand affinity to the receptor was assessed by

575   competitive radioligand binding experiments using ^{125}I-chemerin-9 as radioligand.

576   Displacement binding curves revealed similar IC_{50} values of the labeled (with ^{nat}Ga) and

577   unlabeled (without ^{nat}Ga) DOTA conjugate indicating high affinity. Data are shown as

578   mean ± SEM of three independent experiments normalized to non-competed radioligand

579   binding. **(D)** To assess how the conjugation affects the ligand characteristics, functional

580   and affinity data were obtained accordingly for all five chemerin conjugates (summarized

581   as EC_{50}/IC_{50} values). The Ca^{2+} and binding assays were performed with HEK293a cells

582   stably expressing huCMKLR1 and $G_{\alpha 16}$. All EC_{50}/IC_{50} values were obtained from three

583   independent experiments and are indicated as means ± SD. (green colors indicate more

584   hydrophilic, red more hydrophobic properties of peptides and linker)

585

586   **Figure 3: Comparison of tracer biodistribution by PET imaging.** Representative static

587   PET images were acquired for 30 minutes one hour post-injection of the five ^{68}Ga-labeled

588   DOTA conjugates in a DU4475/A549 tumor model and revealed a differential distribution.

589   Approximately 20 MBq of each tracer were injected intravenously. **(A)** Predominant renal

590   excretion of the hydrophilic tracer ^{68}Ga-DOTA-TTDS-CG34 is indicated by a pronounced

591   kidney signal (yellow arrow). **(B-C)** The more hydrophobic linkers AHX and KCap led to

592   less kidney signal, but more distinct DU4475 uptake (white arrows). **(D)** Beside the kidney

593   uptake, ^{68}Ga-DOTA-ADX-CG34 induced an increased liver signal (red arrow). **(E)** ^{68}Ga-

594   DOTA-AHX-CG36 showed a comparable kidney and liver uptake, but less accumulation

595   in the DU4475 tumor.

596

597   **Figure 4: PET/MR imaging and biodistribution study with CMKLR1-targeted,**

598   **chemerin-based tracers ^{68}Ga-DOTA-KCap-CG34 and ^{68}Ga-DOTA-ADX-CG34.**

599   Representative static PET images were acquired for 30 minutes one and two hours post-

600   injection (p.i.) of 20 MBq ^{68}Ga-labeled conjugate in DU4475 (target-positive) and A549

601   (negative) tumor model (upper panel). For quantitative analysis of tracer biodistribution,

602   10 MBq of the tracer was injected intravenously and tissue was analyzed *ex vivo* one or

603   two hours p.i. Values for tracer uptake are indicated as percent injected activity per gram

604   tissue (% IA/g) (lower panel). **(A)** The T2-weighted MRI image clearly shows both tumors

605   on the animal´s shoulders. The PET images reveal ^{68}Ga-DOTA-KCap-CG34 uptake in

606   DU4475 after one hour, which decreased two hours p.i. The A549 tumor accumulated

607   much less activity. Beside tumor uptake, the tracer accumulated in the kidneys after one

608   hour. The quantitative analysis of biodistribution indicates the clear tracer uptake in

609   DU4475 as compared to A549. Predominant renal excretion is represented by a

610   noticeable kidney value (3 ≤ n ≤ 15; mean ± SEM). **(B)** Injection of ^{68}Ga-DOTA-ADX-

611   CG34 resulted in a strong DU4475 and low A549 uptake. In addition, tracer uptake was

612   detected in kidneys and liver. Quantitative analysis of tracer biodistribution after one hour

613   shows a high uptake in DU4475, and less in A549 tumors. Furthermore, the more

614   hydrophobic tracer accumulated in the kidneys, liver and spleen and led to an overall

615   stronger and longer organ accumulation (5 ≤ n ≤ 16; mean ± SEM).

616

617   **Figure 5: PET/MR imaging and biodistribution study along with a blocking**

618   **experiment.** Representative static PET images were acquired for 30 minutes one and

619   two hours p.i. of ^{68}Ga-labeled DOTA-AHX-CG34 conjugate **(A)** without and **(B)** with

620   coinjected 50-fold excess of unlabeled peptide CG34 (200 nmol) in the same animal.

621   20 MBq of the tracer were injected intravenously. PET images show a strong DU4475

622   uptake, which could be completely displaced with excess of non-labeled peptide.

623   Quantitative analysis of tracer biodistribution (10 MBq) one hour p.i. **(C)** without and **(D)**

624   with receptor blocking confirmed mainly the specific tracer uptake in the DU4475 tumor.

625   (6 ≤ n ≤ 13; mean ± SEM)

626   **Tables**

627

628   **Table 1: Biodistribution data and tissue radioactivity ratios of ^{68}Ga-labeled**

629   **chemerin tracers in the DU4475/A549 xenograft model.** Data are presented as

630   mean ± SEM (2 ≤ n ≤ 16) % IA/g of tissue or as a ratio. Blocking studies were performed

631   in the presence of 200 nmol of CG34.

632

31

633

Organ	68Ga-DOTA-AHX-CG34			68Ga-DOTA-KCap-CG34			68Ga-DOTA-ADX-CG34		
	1 h	1 h-blocked	2 h	1 h	1 h-blocked	2 h	1 h	1 h-blocked	2 h
DU4475	5.1 ± 0.5	0.8 ± 0.1	4.9 ± 0.8	4.3 ± 1.0	0.6 ± 0.1	2.9 ± 0.5	6.2 ± 0.5	1.8 ± 0.1	4.2 ± 1.0
A549	3.0 ± 0.3	1.1 ± 0.2	1.4 ± 0.1	2.3 ± 0.4	0.6 ± 0.1	n.d.	2.7 ± 0.4	1.6 ± 0.2	4.5
small intestine	2.1 ± 0.2	0.4 ± 0.0	2.0 ± 0.4	2.3 ± 0.1	0.3 ± 0.1	1.9 ± 0.3	3.8 ± 0.2	1.4 ± 0.2	4.4 ± 2.0
colon	2.7 ± 0.3	0.5 ± 0.0	2.6 ± 0.7	2.4 ± 0.2	0.3 ± 0.0	1.7 ± 0.2	3.2 ± 0.3	1.2 ± 0.1	2.3 ± 0.3
liver	2.4 ± 0.3	0.6 ± 0.0	2.4 ± 0.4	2.2 ± 0.1	0.3 ± 0.0	1.8 ± 0.2	14.2 ± 1.1	10.4 ± 0.9	12.5 ± 1.1
spleen	6.3 ± 0.8	0.8 ± 0.1	5.0 ± 0.5	4.9 ± 0.5	0.5 ± 0.1	4.0 ± 0.6	7.8 ± 0.6	2.3 ± 0.4	5.4 ± 1.0
kidney	6.5 ± 0.9	8.6 ± 1.4	6.6 ± 1.1	5.8 ± 0.9	5.2 ± 0.9	6.5 ± 1.3	10.3 ± 1.7	14.5 ± 3.9	5.5 ± 1.6
heart	1.2 ± 0.1	0.4 ± 0.0	1.1 ± 0.3	1.1 ± 0.1	0.2 ± 0.0	0.8 ± 0.1	2.2 ± 0.2	1.4 ± 0.1	1.2 ± 0.1
blood	1.2 ± 0.4	0.8 ± 0.1	0.4 ± 0.1	0.6 ± 0.1	0.5 ± 0.1	0.2 ± 0.0	2.8 ± 0.7	3.2 ± 0.3	0.8 ± 0.1
lung	4.2 ± 0.5	1.0 ± 0.1	2.8 ± 0.3	1.7 ± 0.1	0.5 ± 0.1	1.2 ± 0.1	7.1 ± 0.7	3.4 ± 0.2	3.9 ± 0.4
muscle	0.7 ± 0.1	0.2 ± 0.0	0.5 ± 0.1	0.6 ± 0.1	0.2 ± 0.1	0.4 ± 0.1	1.1 ± 0.1	0.6 ± 0.1	0.6 ± 0.1
femur	0.8 ± 0.1	0.2 ± 0.0	0.7 ± 0.1	0.6 ± 0.1	0.2 ± 0.1	0.5 ± 0.1	1.3 ± 0.2	0.7 ± 0.1	0.7 ± 0.1
stomach	1.7 ± 0.2	0.4 ± 0.0	1.3 ± 0.1	1.4 ± 0.1	0.3 ± 0.1	1.1 ± 0.2	2.2 ± 0.2	1.1 ± 0.1	1.5 ± 0.2
pancreas	1.0 ± 0.1	0.3 ± 0.0	0.8 ± 0.1	0.9 ± 0.1	0.2 ± 0.0	0.7 ± 0.1	1.7 ± 0.2	0.8 ± 0.1	1.1 ± 0.1
tumor-to-blood	5.9 ± 0.7	1.0 ± 0.1	13.3 ± 3.0	7.3 ± 1.6	1.3 ± 0.3	18.2 ± 3.4	3.0 ± 0.3	0.6 ± 0.1	5.7 ± 1.1
tumor-to-liver	2.3 ± 0.2	1.2 ± 0.0	2.2 ± 0.5	2.1 ± 0.5	1.8 ± 0.3	1.8 ± 0.4	0.4 ± 0.0	0.2 ± 0.0	0.3 ± 0.1
tumor-to-kidney	0.9 ± 0.1	0.1 ± 0.0	0.7 ± 0.1	0.7 ± 0.1	0.1 ± 0.0	0.6 ± 0.1	0.8 ± 0.1	0.2 ± 0.0	0.8 ± 0.2
tumor-to-pancreas	5.6 ± 0.7	2.9 ± 0.2	6.2 ± 1.3	4.9 ± 1.2	3.7 ± 0.5	4.3 ± 0.9	3.9 ± 0.3	2.3 ± 0.2	3.9 ± 0.7
tumor-to-muscle	8.5 ± 1.0	4.4 ± 0.3	11.4 ± 2.4	8.9 ± 2.3	4.3 ± 0.9	7.2 ± 1.2	6.3 ± 0.5	3.3 ± 0.3	7.2 ± 1.2

634

References

1.	Sai KKS, Zachar Z, Bingham PM, Mintz A. Metabolic PET Imaging in Oncology. AJR Am J Roentgenol. 2017; 209: 270-6.

2.	!!! INVALID CITATION !!! [2-4].

3.	Turker NS, Heidari P, Kucherlapati R, Kucherlapati M, Mahmood U. An EGFR targeted PET imaging probe for the detection of colonic adenocarcinomas in the setting of colitis. Theranostics. 2014; 4: 893-903.

4.	Lutje S, Heskamp S, Cornelissen AS, Poeppel TD, van den Broek SA, Rosenbaum-Krumme S, et al. PSMA Ligands for Radionuclide Imaging and Therapy of Prostate Cancer: Clinical Status. Theranostics. 2015; 5: 1388-401.

5.	Niu G, Chen X. Why integrin as a primary target for imaging and therapy. Theranostics. 2011; 1: 30-47.

6.	Nieto Gutierrez A, McDonald PH. GPCRs: Emerging anti-cancer drug targets. Cell Signal. 2018; 41: 65-74.

7.	Insel PA, Sriram K, Wiley SZ, Wilderman A, Katakia T, McCann T, et al. GPCRomics: GPCR Expression in Cancer Cells and Tumors Identifies New, Potential Biomarkers and Therapeutic Targets. Front Pharmacol. 2018; 9: 431.

8.	Chames P, Van Regenmortel M, Weiss E, Baty D. Therapeutic antibodies: successes, limitations and hopes for the future. Br J Pharmacol. 2009; 157: 220-33.

9.	Fani M, Maecke HR, Okarvi SM. Radiolabeled peptides: valuable tools for the detection and treatment of cancer. Theranostics. 2012; 2: 481-501.

10.	Kamath AV. Translational pharmacokinetics and pharmacodynamics of monoclonal antibodies. Drug Discov Today Technol. 2016; 21-22: 75-83.

11.	Zhao N, Qin Y, Liu H, Cheng Z. Tumor-Targeting Peptides: Ligands for Molecular Imaging and Therapy. Anticancer Agents Med Chem. 2018; 18: 74-86.

12.	Kubota A, Yamada Y, Kagimoto S, Shimatsu A, Imamura M, Tsuda K, et al. Identification of somatostatin receptor subtypes and an implication for the efficacy of somatostatin analogue SMS 201-995 in treatment of human endocrine tumors. J Clin Invest. 1994; 93: 1321-5.

13.	Hoyer D, Bell GI, Berelowitz M, Epelbaum J, Feniuk W, Humphrey PP, et al. Classification and nomenclature of somatostatin receptors. Trends Pharmacol Sci. 1995; 16: 86-8.

14.	Reubi JC. Somatostatin and other Peptide receptors as tools for tumor diagnosis and treatment. Neuroendocrinology. 2004; 80 Suppl 1: 51-6.

15.	Binderup T, Knigge U, Mellon Mogensen A, Palnaes Hansen C, Kjaer A. Quantitative gene expression of somatostatin receptors and noradrenaline transporter underlying scintigraphic results in patients with neuroendocrine tumors. Neuroendocrinology. 2008; 87: 223-32.

16.	Shi W, Johnston CF, Buchanan KD, Ferguson WR, Laird JD, Crothers JG, et al. Localization of neuroendocrine tumours with [111In] DTPA-octreotide scintigraphy (Octreoscan): a comparative study with CT and MR imaging. QJM. 1998; 91: 295-301.

17.	Nauck C, Ivancevic V, Emrich D, Creutzfeldt W. 111In-pentetreotide (somatostatin analogue) scintigraphy as an imaging procedure for endocrine gastro-entero-pancreatic tumors. Z Gastroenterol. 1994; 32: 323-7.

18.	Johnbeck CB, Knigge U, Kjaer A. PET tracers for somatostatin receptor imaging of neuroendocrine tumors: current status and review of the literature. Future Oncol. 2014; 10: 2259-77.

19.	Gabriel M, Decristoforo C, Kendler D, Dobrozemsky G, Heute D, Uprimny C, et al. 68Ga-DOTA-Tyr3-octreotide PET in neuroendocrine tumors: comparison with somatostatin receptor scintigraphy and CT. J Nucl Med. 2007; 48: 508-18.

33

681   20.   Kwekkeboom DJ, Bakker WH, Kooij PP, Konijnenberg MW, Srinivasan A, Erion JL, et al. [177Lu-
682   DOTAOTyr3]octreotate: comparison with [111In-DTPAo]octreotide in patients. Eur J Nucl Med. 2001; 28:
683   1319-25.

684   21.   Yoshimura T, Oppenheim JJ. Chemokine-like receptor 1 (CMKLR1) and chemokine (C-C motif)
685   receptor-like 2 (CCRL2); two multifunctional receptors with unusual properties. Exp Cell Res. 2011; 317:
686   674-84.

687   22.   Ernst MC, Haidl ID, Zuniga LA, Dranse HJ, Rourke JL, Zabel BA, et al. Disruption of the chemokine-
688   like receptor-1 (CMKLR1) gene is associated with reduced adiposity and glucose intolerance.
689   Endocrinology. 2012; 153: 672-82.

690   23.   Mattern A, Zellmann T, Beck-Sickinger AG. Processing, signaling, and physiological function of
691   chemerin. IUBMB Life. 2014; 66: 19-26.

692   24.   Ferland DJ, Watts SW. Chemerin: A comprehensive review elucidating the need for
693   cardiovascular research. Pharmacol Res. 2015; 99: 351-61.

694   25.   Pachynski RK, Zabel BA, Kohrt HE, Tejeda NM, Monnier J, Swanson CD, et al. The
695   chemoattractant chemerin suppresses melanoma by recruiting natural killer cell antitumor defenses. J
696   Exp Med. 2012; 209: 1427-35.

697   26.   Parolini S, Santoro A, Marcenaro E, Luini W, Massardi L, Facchetti F, et al. The role of chemerin in
698   the colocalization of NK and dendritic cell subsets into inflamed tissues. Blood. 2007; 109: 3625-32.

699   27.   Kumar JD, Kandola S, Tiszlavicz L, Reisz Z, Dockray GJ, Varro A. The role of chemerin and
700   ChemR23 in stimulating the invasion of squamous oesophageal cancer cells. Br J Cancer. 2016; 114:
701   1152-9.

702   28.   Tummler C, Snapkov I, Wickstrom M, Moens U, Ljungblad L, Maria Elfman LH, et al. Inhibition of
703   chemerin/CMKLR1 axis in neuroblastoma cells reduces clonogenicity and cell viability in vitro and impairs
704   tumor growth in vivo. Oncotarget. 2017; 8: 95135-51.

705   29.   Li JJ, Yin HK, Guan DX, Zhao JS, Feng YX, Deng YZ, et al. Chemerin suppresses hepatocellular
706   carcinoma metastasis through CMKLR1-PTEN-Akt axis. Br J Cancer. 2018; 118: 1337-48.

707   30.   Kumar JD, Aolymat I, Tiszlavicz L, Reisz Z, Garalla HM, Beynon R, et al. Chemerin acts via CMKLR1
708   and GPR1 to stimulate migration and invasion of gastric cancer cells: putative role of decreased TIMP-1
709   and TIMP-2. Oncotarget. 2019; 10: 98-112.

710   31.   Greenwood FC, Hunter WM, Glover JS. The Preparation of I-131-Labelled Human Growth
711   Hormone of High Specific Radioactivity. Biochem J. 1963; 89: 114-23.

712   32.   Wittamer V, Gregoire F, Robberecht P, Vassart G, Communi D, Parmentier M. The C-terminal
713   nonapeptide of mature chemerin activates the chemerin receptor with low nanomolar potency. J Biol
714   Chem. 2004; 279: 9956-62.

715   33.   Bandholtz S, Wichard J, Kuhne R, Grotzinger C. Molecular evolution of a peptide GPCR ligand
716   driven by artificial neural networks. PLoS One. 2012; 7: e36948.

717   34.   Fani M, Del Pozzo L, Abiraj K, Mansi R, Tamma ML, Cescato R, et al. PET of somatostatin receptor-
718   positive tumors using 64Cu- and 68Ga-somatostatin antagonists: the chelate makes the difference. J Nucl
719   Med. 2011; 52: 1110-8.

720   35.   Zhang X, Wang B, Zhao N, Tian Z, Dai Y, Nie Y, et al. Improved Tumor Targeting and Longer
721   Retention Time of NIR Fluorescent Probes Using Bioorthogonal Chemistry. Theranostics. 2017; 7: 3794-
722   802.

723   36.   Chen Y, Pullambhatla M, Banerjee SR, Byun Y, Stathis M, Rojas C, et al. Synthesis and biological
724   evaluation of low molecular weight fluorescent imaging agents for the prostate-specific membrane
725   antigen. Bioconjug Chem. 2012; 23: 2377-85.

726   37.   Mankoff DA, Link JM, Linden HM, Sundararajan L, Krohn KA. Tumor receptor imaging. J Nucl
727   Med. 2008; 49 Suppl 2: 149S-63S.

728   38.   Ginj M, Maecke HR. Radiometallo-labeled peptides in tumor diagnosis and therapy. Met Ions Biol
729   Syst. 2004; 42: 109-42.

730   39.   Kennedy AJ, Davenport AP. International Union of Basic and Clinical Pharmacology CIII: Chemerin
731   Receptors CMKLR1 (Chemerin1) and GPR1 (Chemerin2) Nomenclature, Pharmacology, and Function.
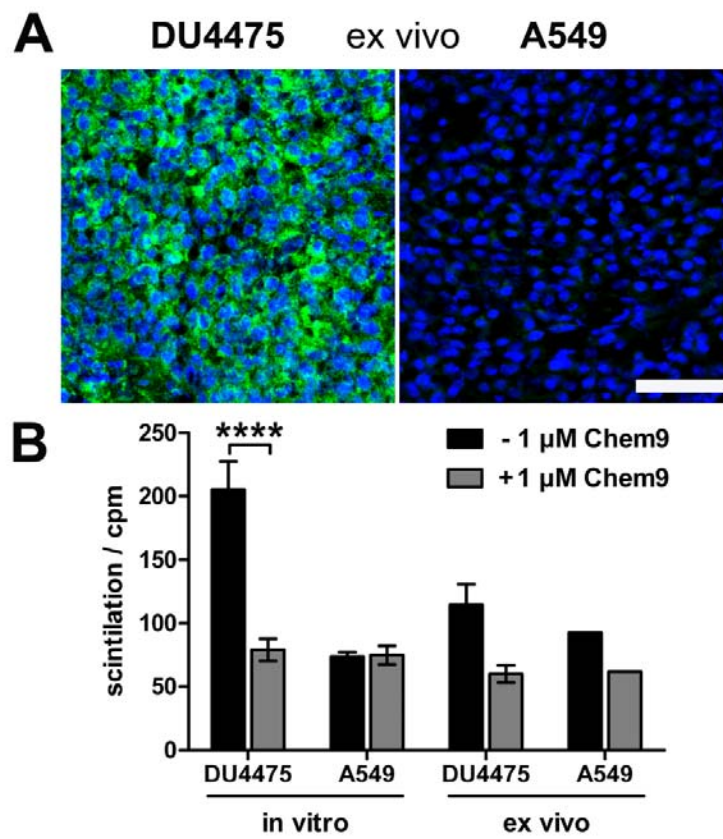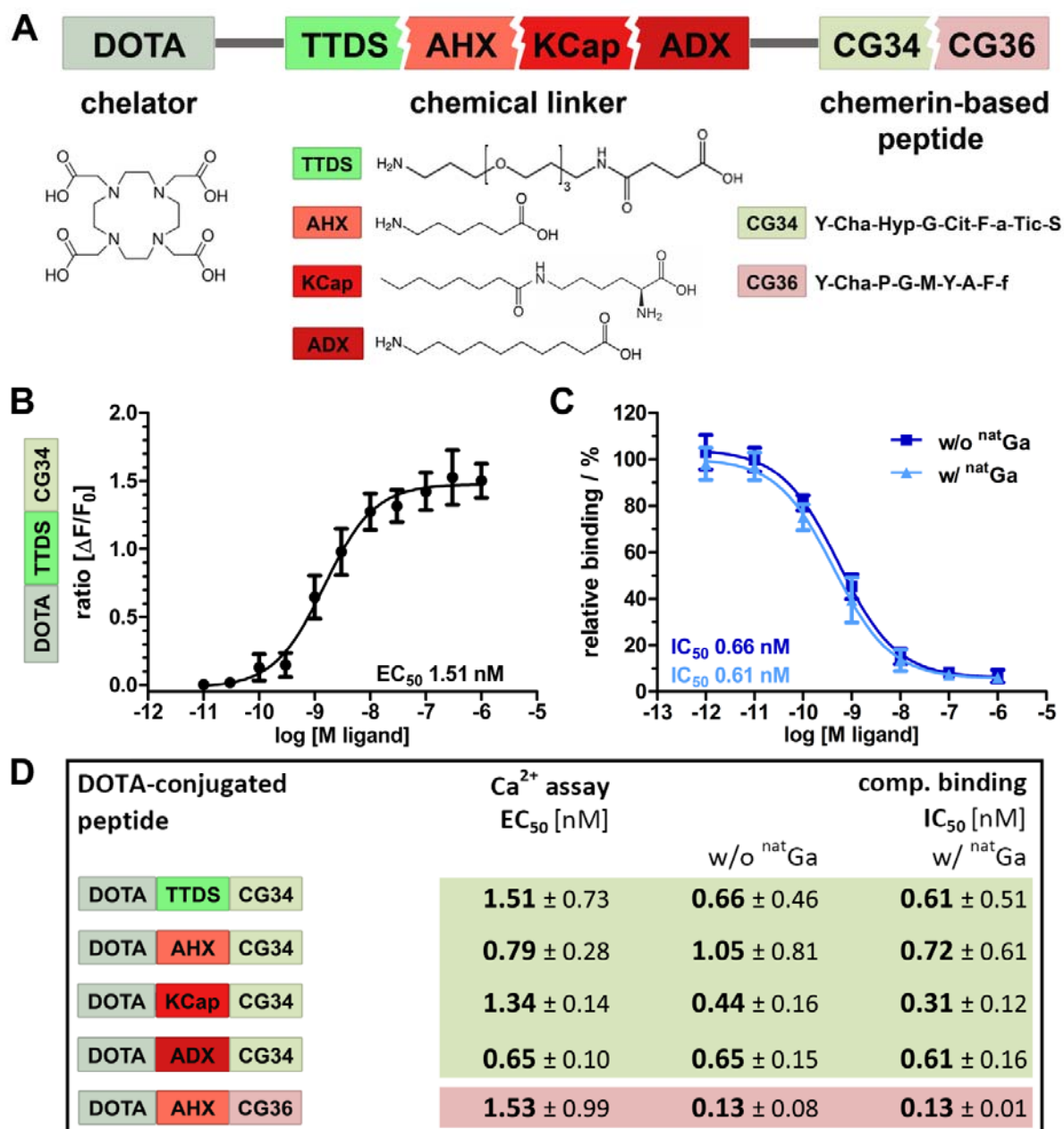732   Pharmacol Rev. 2018; 70: 174-96.
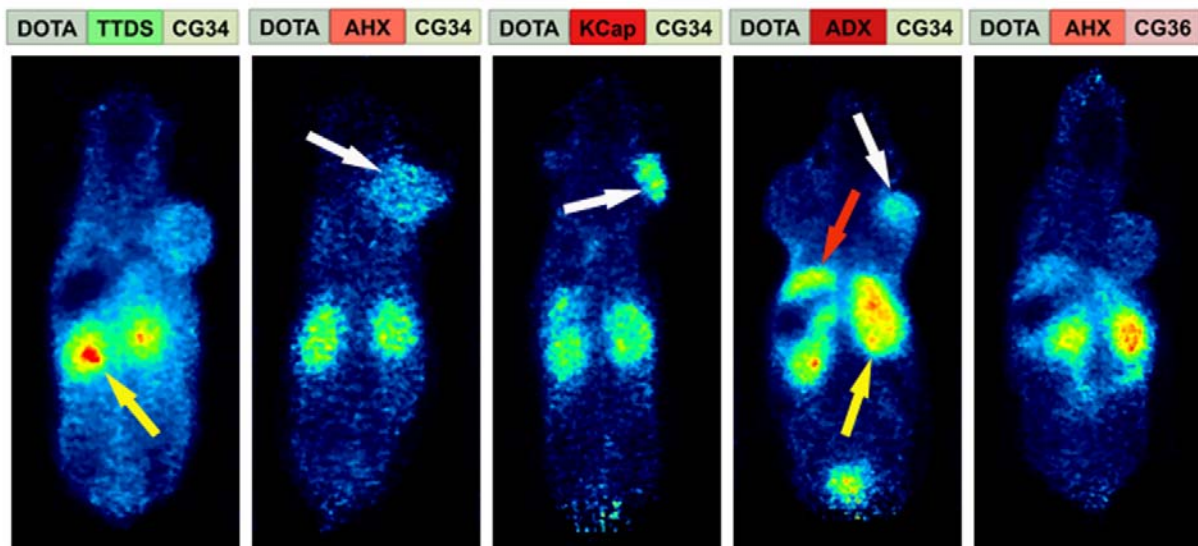
733
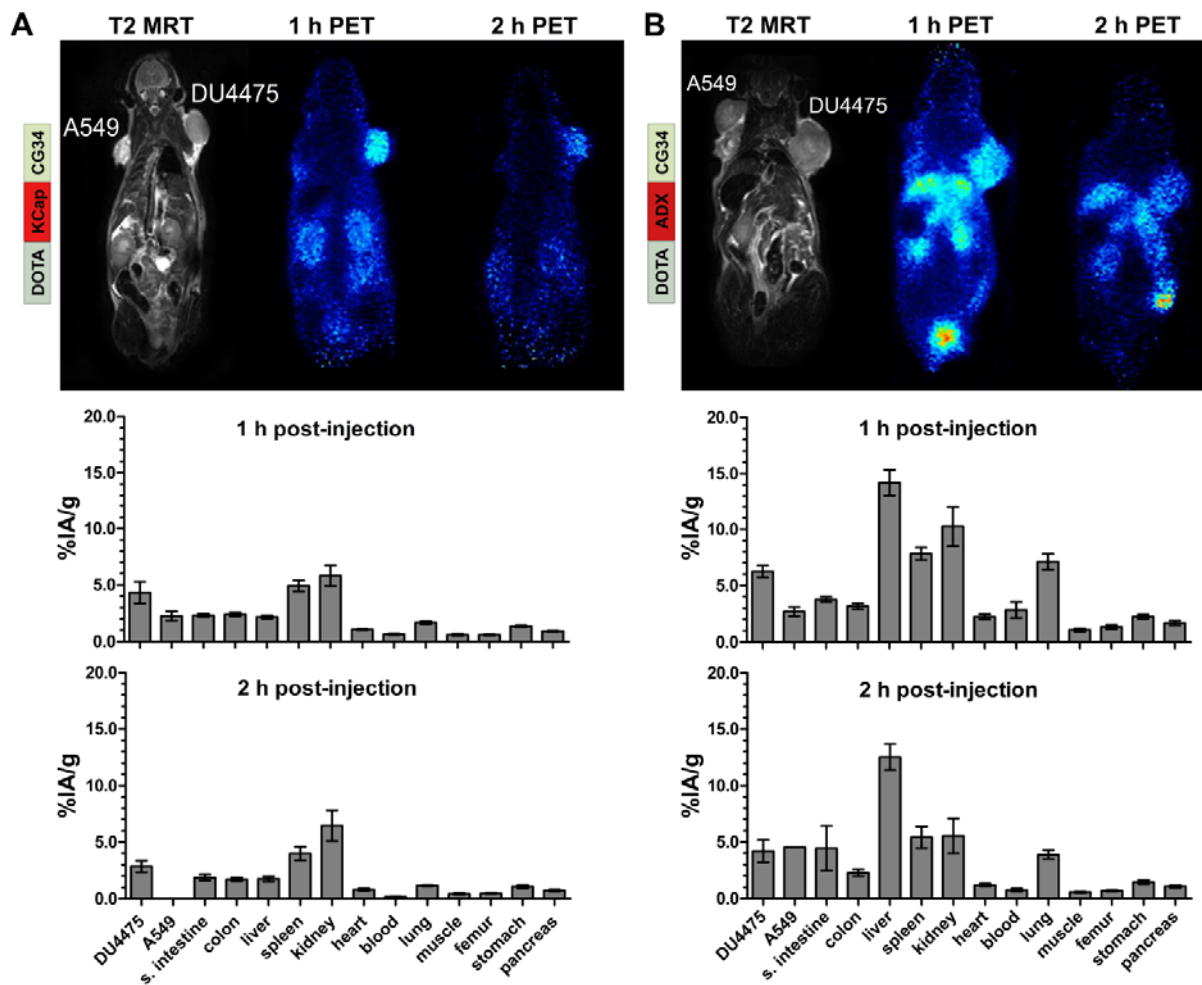
734

Figure 1

36

Figure 2

Figure 3

Figure 4

Figure 5